Published in final edited form as:

Nature. 2014 June 26; 510(7506): 556–559. doi:10.1038/nature13295.

BRCA1 controls homologous recombination at Tus/*Ter*-stalled mammalian replication forks

Nicholas A. Willis[1], **Gurushankar Chandramouly**[1,2], **Bin Huang**[1,3], **Amy Kwok**[1,4], **Cindy Follonier**[5], **Chuxia Deng**[6], and **Ralph Scully**[1,7]

[1]Beth Israel Deaconess Medical Center and Harvard Medical School, 330 Brookline Ave, Boston, MA 02215

[5]Princeton University, 101 Lewis Thomas Laboratory, Washington Road, Princeton, NJ 08544

[6]NIDDK, National Institutes of Health, Building 10, Room 9N105, 10 Center Dr., Bethesda, MD 20814

Abstract

Replication fork stalling can promote genomic instability, predisposing to cancer and other diseases[1–3]. Stalled replication forks may be processed by sister chromatid recombination (SCR), generating error-free or error-prone homologous recombination (HR) outcomes[4–8]. In mammalian cells, a long-standing hypothesis proposes that the major hereditary breast/ovarian cancer predisposition gene products, BRCA1 and BRCA2, control HR/SCR at stalled replication forks[9]. Although BRCA1 and BRCA2 affect replication fork processing[10–12], direct evidence that *BRCA* genes regulate HR at stalled chromosomal replication forks is lacking due to a dearth of tools for studying this process. We report that the *Escherichia coli* Tus/*Ter* complex[13–16] can be engineered to induce site-specific replication fork stalling and chromosomal HR/SCR in mammalian cells. Tus/*Ter*-induced HR entails processing of bidirectionally arrested forks. We find that the BRCA1 C-terminal tandem BRCT repeat and regions of BRCA1 encoded by exon 11—two BRCA1 elements implicated in tumor suppression—control Tus/*Ter*-induced HR. Inactivation of either BRCA1 or BRCA2 increases the absolute frequency of “long-tract” gene conversions at Tus/*Ter*-stalled forks—an outcome not observed in response to a restriction endonuclease-mediated chromosomal double strand break (DSB). Therefore, HR at stalled forks is regulated differently from HR at DSBs arising independently of a fork. We propose that aberrant long-tract HR at stalled replication forks contributes to genomic instability and breast/ovarian cancer predisposition in *BRCA* mutant cells.

[7]Correspondence and requests for materials should be addressed to rscully@bidmc.harvard.edu.
[2]Current address: Temple University, 1801 N Broad St, Philadelphia, Pennsylvania 19122
[3]Current address: Brandeis University, 415 South St, Waltham, MA 02453
[4]Current address: University of Massachusetts Medical School, 55 Lake Avenue North Worcester, MA 01655

Author Contributions

N.A.W., G.C. and R.S. designed experiments. N.A.W., G.C., B.H. and A.K. performed experiments. C.F. provided expert advice on execution of 2D gel electrophoresis experiments. C.D. generated *Brca1* exon 11 conditional ES cells. N.A.W. analyzed the data. N.A.W. and R.S wrote the manuscript.

The authors declare that they have no competing financial interests.

Tus binds the 23-bp *Ter* site to induce polar replication fork arrest in *E. coli*[13–16]. To determine whether Tus/*Ter* can arrest mammalian replisomes, we introduced six *TerB* sites into a plasmid containing the Epstein Barr Nuclear Antigen 1 (EBNA1)-binding origin of replication ("p6x*Ter*Ori", Fig. 1a). EBNA1 recruits mammalian replication factors, mediating predominantly unidirectional plasmid replication, due to a replication block at EBNA1-bound "FR" repeats[17]. In p6x*Ter*Ori, the major clockwise fork approaches the "non-permissive" (fork-stalling) face of Tus/*Ter* (Fig. 1a). We used two-dimensional DNA gel electrophoresis (2DGE) with Southern blotting to visualize replication through 6x*Ter*. Transfection of 293E cells, which express EBNA1[18], with p6x*Ter*Ori and control empty vector revealed plasmid replication intermediates (arc "A", Fig. 1b). Co-transfection of p6x*Ter*Ori and wild-type (wt) myc-tagged Tus revealed site-specific stalling of the clockwise fork (spot "B", Fig. 1b, 1c; Extended Data Fig. 1). TusH144A, a *Ter* binding-impaired mutant[16], induced minimal fork stalling. 6x*Ter* in the "permissive" orientation ("6xREV*Ter*", Fig 1b) also mediated Tus-dependent stalling of the clockwise fork, albeit less efficiently than non-permissive 6x*Ter* (Fig. 1b and 1c). The FR/EBNA1 replication block is incomplete[19]. A weaker Tus/*Ter*-dependent double-Y spot ("C", Fig. 1b), reflects bidirectional fork arrest at 6x*Ter*. (We estimate the FR/EBNA1 and Tus/6x*Ter* replication block efficiencies as ~70%; Extended Data Fig. 2). Thus, Tus/*Ter* mediates bidirectional site-specific arrest of mammalian replication forks.

To determine whether Tus/*Ter* induces HR/SCR at a defined chromosomal locus in mammalian cells, we placed 6x*Ter* in an HR reporter of short- and long-tract gene conversion (STGC and LTGC) between sister chromatids[20]. Duplication of a red fluorescent protein (*RFP*) cassette distinguishes LTGC (length ≥1252 bp; GFP^+RFP^+) from STGC (length <1252 bp; GFP^+RFP^-; Fig. 2a)[20]. 6x*Ter* abuts an I-SceI restriction site, interrupting an enhanced green fluorescent protein gene ("6x*Ter*-I-SceI-*GFP*", Fig. 2a). Recombination of the stalled left-hand fork (Fig. 2a) with the 5′-truncated *GFP* copy ("Tr-*GFP*") of the sister chromatid generates wt*GFP*. If chromosomal fork arrest were bidirectional, this could produce a two-ended break, generating predominantly STGCs (Fig. 2a, Extended Data Fig. 3a)[20]. In contrast, unidirectional fork arrest with one-ended breaks would favor LTGC, and any STGCs arising from one-ended breaks would necessarily be terminated by non-canonical mechanisms (Extended Data Fig. 3b)[20].

We targeted the 6x*Ter*/HR reporter as a single copy to the *ROSA26* locus of mouse embryonic stem (ES) cell line 11CO/47T ("$Brca1^{fl/BRCT}$")[20]. $Brca1^{BRCT}$ encodes a C-terminal truncated protein; the BRCT-encoding elements of $Brca1^{fl}$ can be conditionally deleted (generating "$Brca1^{\Delta}$")[20]. Indeed, wtTus, but not TusH144A, induced HR within 6x*Ter*/HR $Brca1^{fl/BRCT}$ cells, the major HR product being STGC (Fig. 2b). wtTus failed to induce HR in $Brca1^{fl/BRCT}$ cells containing a *ROSA26*-targeted HR reporter lacking the *Ter* array (Fig. 2b)[20]. Thus, Tus/*Ter*-induced chromosomal HR requires cognate Tus-*Ter* binding. The ratio LTGC/Total HR, a measure of the probability that HR resolves as LTGC, was ~7% in three independent Tus-transfected clones (Fig. 2c; Extended Data Fig. 4a). Three additional independent clones of $Brca1^{fl/BRCT}$ ES cells, each containing a single-copy randomly integrated chromosomal 6x*Ter*/HR reporter, behaved similarly (Extended Data Fig. 4b). The predominance of STGC and the consistent results at different loci suggested

that Tus/*Ter*-induced HR entails bidirectional fork arrest (Extended Data Fig. 3a). We resolved this definitively by Southern blot analysis of Tus/*Ter*-induced STGCs. Unidirectional fork arrest/breakage (Extended Data Fig. 3b) could produce a one-ended break, generating STGC products of variable size[20]. In contrast, bidirectional fork arrest (Fig. 2a, Extended Data Fig. 3a) could produce a two-ended break, with STGC termination by annealing. This would generate STGC products of fixed size, resembling the parental reporter but lacking the 6x*Ter* array or I-SceI site (Fig 2a)[20]. Indeed, 44/44 Tus/*Ter*-induced STGCs in 6x*Ter*/HR reporter *Brca1*$^{fl/BRCT}$ cells revealed this latter structure (Fig. 2d). As expected, I-SceI-induced HR behaved similarly (Fig. 2d). A second arrested fork (right-hand fork, Fig. 2a) must provide the homologous second end during Tus/*Ter*-induced STGC. Therefore, Tus/*Ter*-induced STGC is the product of bidirectional replication fork arrest. Overall I-SceI-induced HR in *Brca1*$^{fl/BRCT}$ 6x*Ter*/HR reporter cells was ~20% of that in isogenic *ROSA26*-targeted *Brca1*$^{fl/BRCT}$ HR reporter cells, which differ only by the lack of a 6x*Ter* array (data not shown)[20]. The reasons for this difference are unclear.

To investigate further the non-polar behavior of Tus/*Ter* in mammalian HR, we studied the Tus mutant F140A that binds duplex *Ter* with higher affinity than wtTus but is defective for the *Ter* C-6 base-flipping “locking” mechanism that contributes to polar fork arrest in *E. coli*[16]. TusF140A induced higher levels of HR than wtTus in 6x*Ter*/HR *Brca1*$^{fl/BRCT}$ cells (Extended Data Fig. 4c and 4d), showing that the C-6 “lock” is dispensable for Tus/*Ter*-induced HR in mammalian cells. This might be explained by the different polarities of the *E. coli* DnaB and vertebrate MCM replicative helicases. *Ter* C-6 is located on the leading strand of the fork approaching the non-permissive end of *Ter*. Unlike DnaB, which translocates along the lagging strand, the MCM helicase translocates along the leading strand and might occlude *Ter* C-6 within its barrel, thereby denying Tus access to the C-6 lock mechanism. To determine the minimal number of Tus/*Ter* complexes needed for HR induction, we generated reporters containing 3, 2 or 1 *Ter* sites (Extended Data Fig. 4e). We targeted each, in parallel, as a single copy to the *ROSA26* locus of *Brca1*$^{fl/BRCT}$ ES cells and found that a minimum of 3 *Ter* sites is required for robust Tus-induced HR (Extended Data Fig. 4f). We inverted the 6x*Ter* array orientation to generate a “6xREV*Ter*/HR” reporter. When targeted as a single copy to the *ROSA26* locus of *Brca1*$^{fl/BRCT}$ ES cells, this reporter supported Tus-induced HR as robustly as the 6x*Ter*/HR reporter (Extended Data Fig. 4f). Our findings do not exclude a polar component to Tus/*Ter*-induced fork stalling on a mammalian chromosome but this polarity, if present, is relative not absolute.

Interstrand DNA cross-link repair of plasmids replicating in *Xenopus laevis* egg extracts entails endonucleolytic attack of bidirectionally stalled forks[21]. Interestingly, Tus/*Ter*-induced HR was suppressed by depletion of the endonuclease scaffold Slx4/FancP[22,23] to a greater extent than I-SceI-induced HR (Extended Data Fig. 5), suggesting that Slx4 contributes specifically to Tus/*Ter*-induced HR. However, it is not clear whether Slx4 mediates endonucleolytic attack of stalled forks during Tus/*Ter*-induced HR. Work in *Schizosaccharomyces pombe* suggests that alternative mechanisms, such as template switching, could mediate HR at stalled mammalian forks[7].

To determine whether BRCA1 regulates HR at stalled replication forks, we transduced 6x*Ter*/HR *Brca1*$^{fl/BRCT}$ cells with adeno-Cre and screened for wt*Brca1* loss (Fig. 3a). The

resulting *Brca1*$^{\Delta/BRCT}$ cells are viable hypomorphs with growth characteristics similar to *Brca1*$^{fl/BRCT}$ cells[20]. We studied Tus-induced HR in three independent Cre-treated clones of each genotype (Fig. 3). Surprisingly, Tus-induced STGC in 6x*Ter*/HR *Brca1*$^{\Delta/BRCT}$ cells showed no reduction compared to *Brca1*$^{fl/BRCT}$ cells, but LTGC was elevated 2-fold (Fig. 3b). Correspondingly, the probability of engaging LTGC during Tus/*Ter*-induced HR was doubled to ~15% (Fig. 3b). Consistent with our recent findings, I-SceI-induced HR in 6x*Ter*/HR *Brca1*$^{\Delta/BRCT}$ cells was diminished and biased in favor of LTGC (Fig. 3b)[20]. Southern analysis of Tus/*Ter*-induced STGC and LTGC products in 6x*Ter*/HR *Brca1*$^{\Delta/BRCT}$ cells revealed patterns similar to *Brca1*$^{fl/BRCT}$ cells (Extended Data Fig. 6). However, in *Brca1*$^{\Delta/BRCT}$ cells, 6/41 (15%) Tus/*Ter*-induced STGC and 3/15 (20%) LTGC clones retained an additional copy of the parental reporter (Extended Data Fig. 6). This was not separable by recloning, suggesting that it was retained by nondisjunction. 4/41 (9.8%) I-SceI-induced STGC *Brca1*$^{\Delta/BRCT}$ clones revealed nondisjunction; thus, nondisjunction is not specific to Tus/*Ter*-induced HR. The fact that the donor sister was unaltered during LTGC excludes crossing-over as a cause of the LTGC outcome in these clones[24,25].

We asked whether Brca1 domains additional to the BRCT repeat regulate Tus/*Ter*-induced HR. Indeed, siRNA-mediated Brca1 depletion suppressed STGC but increased LTGC in both *Brca1*$^{fl/BRCT}$ and *Brca1*$^{\Delta/BRCT}$ cells (Extended Data Fig. 7). In Brca1-depleted *Brca1*$^{\Delta/BRCT}$ cells, ~40% of all HR products were LTGCs. More than half of the BRCA1 polypeptide is encoded by exon 11, which is a target of inactivating germ line mutation in hereditary breast/ovarian cancer; exon 11 is also alternatively spliced, generating an in-frame nuclear Δexon11 gene product that retains N-terminal RING domain and C-terminal BRCT functions[26]. To test whether *Brca1* exon 11 regulates Tus/*Ter*-induced HR, we targeted a single copy of the 6x*Ter*/HR reporter to the *ROSA26* locus of mouse *Brca1*$^{fl/Exon11}$ ES cells. The *Brca1*^{Exon11} allele lacks exon 11; exon 11 of *Brca1*^{fl} can be conditionally deleted to generate "*Brca1*$^{\Delta}$" (Fig. 4a)[27]. (*Note*: "fl" and "Δ" denote distinct *Brca1* alleles in the two *Brca1* conditional systems described here.) Following adeno-Cre treatment, we retrieved 6x*Ter*/HR *Brca1*$^{fl/Exon11}$ and 6x*Ter*/HR *Brca1*$^{\Delta/Exon11}$ clones. Each of three independent 6x*Ter*/HR *Brca1*$^{\Delta/Exon11}$ clones revealed reduced Tus/*Ter*-induced STGC but increased absolute frequencies of LTGC in comparison with three independent 6x*Ter*/HR *Brca1*$^{fl/Exon11}$ clones (Fig. 4b). Deletion of *Brca1* exon 11 increased the probability of engaging Tus/*Ter*-induced LTGC ~4-fold to ~30% (Fig. 4b). In contrast, the absolute frequency of I-SceI-induced LTGC was reduced in *Brca1*$^{\Delta/Exon11}$ cells and ~20% of HR products were LTGCs (Fig 4b). Thus, *Brca1* exon 11 contributes to Tus/*Ter*-induced HR both quantitatively and qualitatively.

To determine whether BRCA2/Rad51 regulates Tus/*Ter*-induced HR, we used siRNA to deplete Brca2 or Rad51 during HR induction. Depletion of Brca2 suppressed Tus/*Ter*-induced STGC but elevated LTGC frequencies in both *Brca1*$^{fl/BRCT}$ and *Brca1*$^{\Delta/BRCT}$ cells (Extended Data Fig. 8). In *Brca1*$^{fl/BRCT}$ and *Brca1*$^{\Delta/BRCT}$ cells depleted of Brca2, ~30% and ~50% respectively of all Tus/*Ter*-induced HR products were LTGCs, while the equivalent probabilities for Rad51-depleted cells were ~40% and ~70% (Extended Data Fig. 9). Thus, suppression of LTGC at stalled forks is a shared function of BRCA1, BRCA2 and Rad51. Inhibition of 53BP1 partially reversed defective I-SceI-induced HR in *Brca1*$^{\Delta/BRCT}$ cells, as

expected[20], but did not affect Tus/*Ter*-induced HR in either *Brca1*$^{fl/BRCT}$ or *Brca1*$^{\Delta/BRCT}$ cells (Extended Data Fig. 10). This suggests that BRCA1's functions in Tus/*Ter*-induced and SceI-induced HR are, in part, distinct. LTGC at stalled forks may include pathological responses analogous to break-induced replication in yeast[3,8,28,29]. Our work identifies loss of BRCA1/BRCA2/Rad51-dependent suppression of LTGC at stalled replication forks as a potential contributor to breast/ovarian cancer predisposition.

Methods Summary

A description of the molecular biology methods, cell culture and recombination assays can be found in the full Methods.

Methods

Molecular biology, siRNAs and antibodies

The vector for mammalian expression of myc epitope-tagged, nuclear localized, codon-optimized wild type (wt) Tus (pCMVβ myc-NLS-Tus), vectors p6x*Ter*Ori and p6xrev*Ter*Ori and the *Ter* HR reporters were constructed by conventional cloning methods using a previously described RFP-SCR reporter[31]. *Ter*-containing plasmids were cultivated in JJC33 (*Tus*$^{-}$) strains of *E. coli*. siRNA SMARTpools were purchased from Dharmacon. Cells were lysed in RIPA buffer (50 mM Tris-HCl, pH 8.0, 250 mM NaCl, 0.1% sodium dodecyl sulfate, 1% NP-40 containing protease and phosphatase inhibitors PMSF and Roche complete protease inhibitor tablet). Extracted protein was resolved by 4 –12 % bis-Tris SDS-PAGE (Invitrogen) and analyzed by immunoblotting using the following antibodies; Brca1 (a kind gift of the Baer laboratory, 1:100), beta-tubulin (Abcam ab6046, 1:4,000), beta-actin (Abcam ab8226, 1:10,000), Myc (Abcam ab9106, 1:10,000), hRad51 (aliquot B32, 1:500), and HA (Santa Cruz sc-805, 1:200).

Cell lines and cell culture

Mouse embryonic stem (ES) cells were grown in ES medium on either MEF feeders or gelatinized plates as described previously[31–33]. 10 μg of the 6x*Ter* HR reporter ROSA26 targeting plasmid was linearized by KpnI digest and introduced by electroporation to 1–2 × 10^7 cells and subsequently seeded on 6 cm plates with puromycin-resistant feeders. Plates were supplemented with puromycin (4 μg/ml) 24 hours later and colonies were picked 5–10 days later. *ROSA26* targeted lines were screened for by PCR and verified by Southern blotting[31]. We generated multiple Brca1-deficient ES clones by transient adenovirus-mediated Cre expression. *ROSA26* genotyping primers: *ROSA26-sense*- (cat caa gga aac cct gga cta ctg); *TerBx6 HR reporTer antisense*- (cct cgg cta ggt agg gga tc). Brca1 exon11 status was determined by PCR: *Brca1 5′sense*- (CTG GGT AGT TTG TAA GCA TCC); *Brca1 exon11 antisense*- (CAA TAA ACT GCT GGT CTC AGG C); *Brca1 exon11 sense*- (GGA AAT GGC AAC TTG CCT AG); *Brca1 3′antisense*- (CTG CGA GCA GTC TTC AGA AAG).

Recombination Assays

1.6×10^5 cells were transfected in suspension with 0.5 μg pcDNA3β-myc NLS-I-SceI[34], pcDNA3β-myc NLS-Tus, pcDNA3β-myc NLS-TusH144A, pcDNA3β-myc NLS-TusF140A, or control vector using Lipofectamine 2000 (Invitrogen). GFP^+ and GFP^+RFP^+ frequencies were scored 3 days after transfection by flow cytometry using a Becton Dickinson 5 Laser LSRII in triplicate and values presented corrected for background events and transfection efficiency. Transfection efficiency was measured by parallel transfection with 0.05 μg wt *GFP* expression vector and 0.45μg control vector. Typically 6×10^5 total events were scored per sample. In all figures presented, data represents the mean and standard error of the mean (SEM) of at least three independent experiments. Tus or I-SceI expression vector transfection efficiencies were typically between 50% and 75%, and background levels of HR products typically <0.005% for GFP^+RFP^- and <0.001% for GFP^+RFP^+ (e.g., Extended Data Fig. 2a).

Statistical methods

Each figure legend reports the sample size in terms of number of *replicates* per experiment and number of *experiments* that were analyzed to generate the data shown. For statistical analysis of HR values, the arithmetic mean of triplicate samples was calculated for each independent experiment (i.e., experiments performed on different days) and these single data points for each *experiment* were used to calculate the mean and standard deviation *between* experiments. The standard error of the mean (s.e.m.) was calculated as standard deviation/ √n, where n= *number of experiments* (not number of replicates). For example, if we measured triplicate samples in four different independent experiments, then n=4. Differences between groups were analyzed by Student's two-tailed unpaired *t*-test, assuming unknown variance, using GraphPad Prism v5.0d software. P-values are given in the figure legends. Densitometry of 2D gel data was also analyzed by calculation of arithmetic mean and s.e.m. and analysis by *t*-test. Analysis of trend in Extended Data Fig. 4f was performed by ANOVA using GraphPad Prism v5.0d software, in addition to the *t*-test as described above.

RT-qPCR analysis

RNA from transfected ES cells was extracted by QIAGEN RNeasy Mini Kit (QIAGEN Sciences, Maryland, MD) 2 days post transfection. First-strand cDNA analysis was performed on an ABI 7300 Real time PCR System using Power SYBR Green RNA-toC_T™ 1-Step Kit (Applied Biosystems, Foster City, CA). Taqman probe and primer sets to genotype for *Brca1* were: *Brca1*-Exon-22-23-sense-TTC CGT GGT GAA GGA GCT T; *Brca1*-Exon-22-23-antisense-TGG CTG CAC GAT CAC AAC; *Brca1*-Exon-23-24-sense-GCC TGG ACA GAA GAC AGC A; *Brca1*-Exon-23-24-antisense-CAG TCC CAC ATC ACA AGA CG; *Brca1*-Exon-22-23-taqman probe-FAM-CGC TCA CCC ATG ACA CAG GTG C-BHQ; *Brca1*-Exon-23-24-taqman probe- FAM-TGC ACA GCT GCC CAA TAT CTG GG-BHQ). Conventional SYBR green RT-qPCR assays of *Gapdh* and siRNA-targeted gene was performed. We used the NIH NCI Nucleotide utility to Primer 3 software (Whitehead Institute, MIT) to generate gene-specific primer sequences for mouse *Brca1* and *Gapdh*. We used the NIH NCI Nucleotide utility to generate gene-specific primer sequences

for mouse Slx4, Slx1, Eme1, and Xpf. Primers for RT-PCR: *Brca1*-EXON21-22-sense-ATG AGC TGG AGA GGA TGC TG; *Brca1*-EXON21-22-antisense-CTG GGC AGT TGC TGT CTT CT; *Brca1*-EXON22-23-sense-GGT GCT CAT CTA GTT GTG ATC G; *Brca1*-EXON22-23-antisense-CTG TAC CAG GTA GGC ATC CA; *Brca1*-EXON7-8-sense-AGC CTA GGT GTC CAG CTG TC; *Brca1*-EXON7-8-antisense-CTG CAA TCA CCT GGC TTA GTT; *Brca2-sense-(*tct gcc act gtg aaa aat gc*); Brca2-antisense-(*tca agc tgg gct gaa gat t*); Slx4-sense-(*GTG GGA CGA CTG GAA TGA GG*); Slx4-antisense-(*GCA CCT TTT GGT GTC TCT GG*); Slx1-sense-(*GGA TGG ACC ATG CAG CAA GA*); Slx1-antisense-(*CCA TTC AAA CCG AAG GGC G*); Eme1-sense-(*AGG CCA GAG GAA TGC CTG AA*); Eme1-antisense-(*CCA GTC ATC TCC ATC CTC TAC C*); Xpf-sense-(*TGG TCA GAA TTC AGG TTG GC*); Xpf-antisense-(*TTT CAG GAC GTC AGT CAG CG*). mRNA* was measured in triplicates with a standard curve generated for each gene using cDNA obtained from each sample. The expression level of target genes was normalized to internal *Gapdh*.

293 Cell Transfection and Episome Two-dimensional gel electrophoresis

12×10^6 293HEK or 293E (ATCC CRL-10852) cells were plated per 15 cm dish 1 day prior to transfection. Cells were transfected with 4.5 μg pOri plasmids and 1 μg of control empty vector or pcDNA3β-myc NLS-Tus in antibiotic free media using Lipofectamine2000 reagent, and media changed 24 hours after transfection. 40 hours after transfection, plates were rinsed with 1× PBS and cells washed off the plate with ice-cold PBS, washed again with ice-cold PBS and HIRT extracted as described below. Purified DNA was restriction digested 8–16 hours and run on a 14 × 16 cm 0.4% agar 0.1 μg/ml ethidium bromide 0.5× TBE gel 13 hours in the dark at 40V. First dimension gel slabs were cut out and embedded in the second dimension slab gel (20 × 25 cm 1% agar, 0.5× TBE, 1 μg/ml ethidium bromide) and run at 160V for 7.5 hours in the cold room.

HIRT Episome Extraction from 293 Cells

Plasmid was extracted as published[35]. Briefly, PBS washed 293HEK or 293E cells were lysed in 2.25 mL 0.6% sodium dodecyl sulfate 33 mM Tris-HCl, 6 mM EDTA, 66 g/ml RNase followed by digestion with 0.5 μg Proteinase K for 90 minutes at 37°C. Samples were subject to brief, 20 second, base extraction with 0.75 mL 0.1 M NaOH and proteins precipitated by addition of 1 mL 4.2 M Gu-HCl, 0.9 M Potassium Acetate pH 4.8. Cell debris was pelleted at 39,000×g and supernatant loaded onto a Qiagen Miniprep spin column (QIAGEN Sciences, Maryland, MD). Columns were washed with 0.5 mL Qiagen Buffer PB (5 M Gu-HCl, 30% ethanol, adding 10 mM Tris-HCl pH 6.6) and 0.75 mL Qiagen Buffer PE (10 mM Tris-HCl pH 7.5, 80% ethanol) and plasmid DNA eluted using two volumes of 40 L Qiagen EB buffer.

Southern Blotting

Southern blotting of genomic DNA was performed using *GFP* cDNA or *ROSA26* 5′ probes as described previously[33,34]. For all experiments, including mouse ES cells containing a randomly integrated reporter not at *ROSA26*, clones containing only one intact copy of the reporter were used. Genomic DNA was extracted from confluent ES cells on 6-well plates

(~5–10 × 10^6 cells) using a Puregene DNA Isolation Kit (Gentra Systems). Episomal plasmid DNA was extracted by HIRT extraction described above and Southern blotting performed using random labeled probe produced from the KpnI – HindIII restriction fragment of p6x*Ter*Ori.

Extended Data

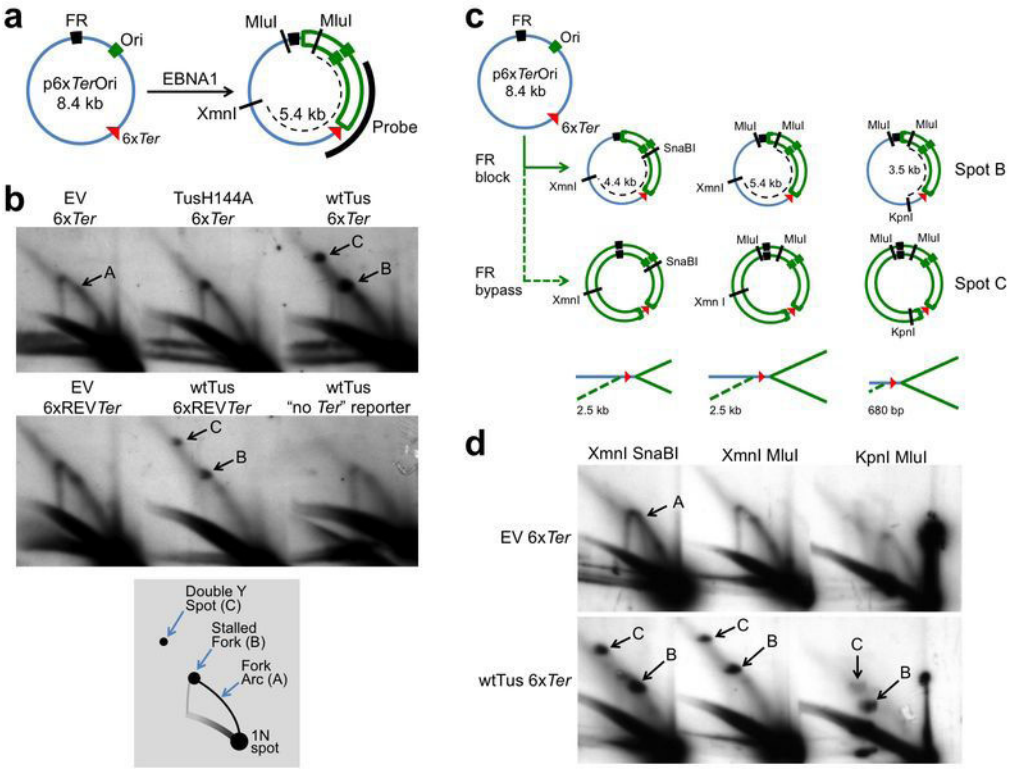

Extended Data Figure 1. Tus/*Ter*-induced replication fork stalling visualized by additional restriction digests

a, Plasmid elements as in Fig. 1a. MluI-XmnI digested plasmid yields linear fragment of 5.4 kb. Probe for Southern blotting indicated by black bar. **b**, Plasmid replication intermediates extracted from 293E cells transiently transfected with 6x*Ter*-containing plasmids or "no *Ter*" control, co-transfected with empty vector (EV), TusH144A or wtTus as shown. All samples are from one experiment (see Source Data 2). Plasmid DNA extracted from 293E cells was digested with XmnI and MluI and analyzed by neutral/neutral 2DGE and Southern blotting. Replication intermediates as described in Fig. 1a. **c**, Predicted replication intermediates generated by Tus/*Ter*-induced replication fork stalling with or without effective FR/EBNA1 replication fork block. Diagrams below plasmid maps show shape of the major Tus/*Ter*-dependent fork arrest species. Green dotted line: predicted additional branch of double Y structure formed by stalling of *counterclockwise* fork at Tus/6x*Ter* when FR/EBNA1 replication block fails. Length of additional branch is shown in each diagram. Note: The relationship between spots B and C will vary according to the length of this additional branch. **d**, Plasmid replication intermediates extracted from 293E cells transiently transfected with 6x*Ter*-containing plasmids and co-transfected with empty vector (EV) or

wtTus as shown. Restriction digests of extracted plasmids as shown. All samples are from one experiment (see Source Data 2). Note: replication fork size and position of stall spot B in relation to replication arc A varies with restriction digest. For example, spot B in KpnI-MluI is close to the 2n linear position, since the Tus/*Ter*-stall site is only ~680 bp from the KpnI site. For the same reason, spots B and C are closely placed in the KpnI-MluI-digested sample.

Note: the relatively weak spot C in the KpnI-MluI digest, which is consistent across multiple experiments, might reflect a proportionately large contribution of ssDNA (reflecting processed lagging strand DNA[21]) to the ~680 bp lagging strand of the stalled counterclockwise fork.

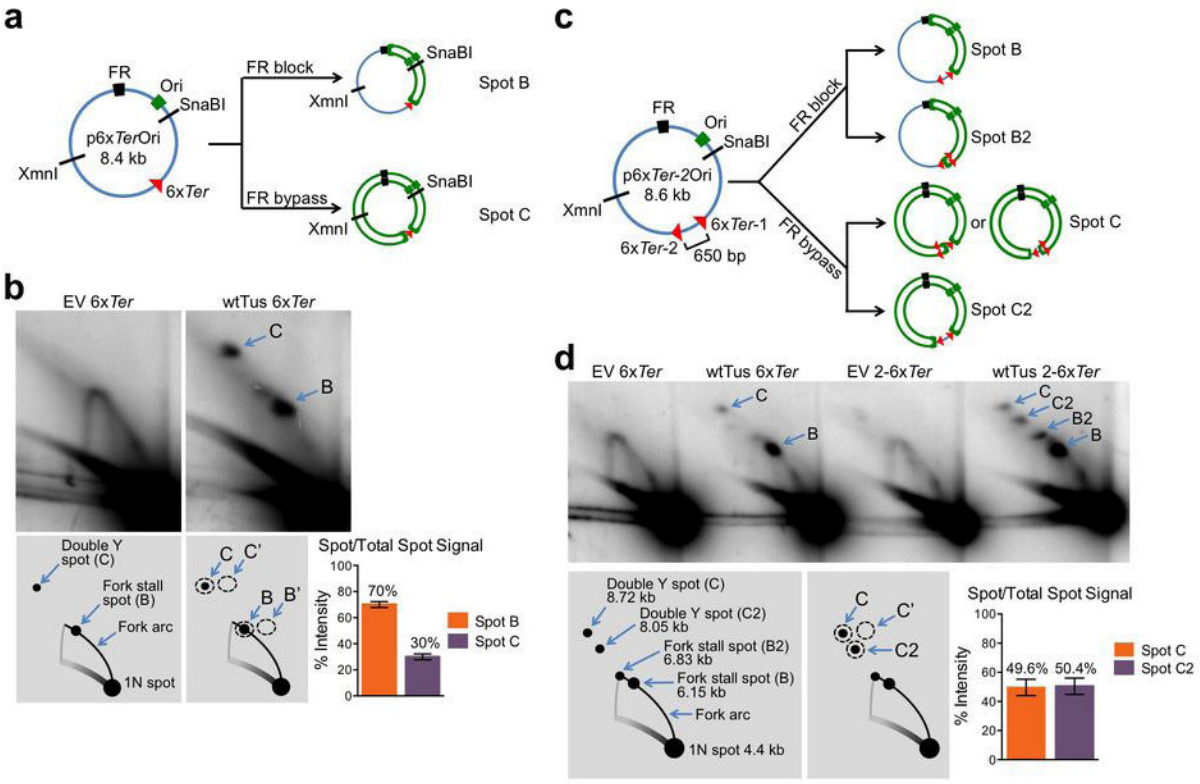

Extended Data Figure 2. Estimation of efficiencies of the FR/EBNA1 and Tus/6x*Ter* replication fork barriers

a, Tus/*Ter*-mediated replication stall structures responsible for spots B and C. The relative abundance of the single stall spot B and the double Y stall spot C can be used to calculate the efficiency of the FR/EBNA1 replication fork barrier. **b**, Phosphorimager analysis of twelve independent Southern blot experiments (method described in Fig. 1b, see Source Data 3). Note: some images shown in Source Data 3 were also used in other figures. Areas B, B′, C and C’ are the same shape and size *within* individual panels. Size and shape of each area varies *between* panels. B: stall spot B. B′: background gel signal of same area as B. C: stall spot C. C’: background gel signal of same area as C. Relative intensity of spot B/B+C estimates the stalling efficiency at FR/EBNA1 and is calculated as:

$$(\mathrm{B}-\mathrm{B}')/(\mathrm{B}+\mathrm{C}-\mathrm{B}'-\mathrm{C}')\times 100\%.$$

The stalling efficiency at FR/EBNA1 is therefore 70% ± 2.2% (s.e.m.).
Relative intensity of spot C is calculated as:

$$(\mathrm{C}-\mathrm{C}')/(\mathrm{B}+\mathrm{C}-\mathrm{B}'-\mathrm{C}')\times 100\%.$$

c, Structure of p6x*Ter*-2Ori plasmid. Stalled replication intermediates depict different combinations of FR/EBNA1 block/bypass and Tus/6x*Ter* block/bypass. Spots B and B2 are defined as in the diagram. Spots C and C2 result from FR/EBNA1 bypass. Spot C2 requires successful arrest at both of the 6x*Ter* arrays. Spot C results from bypass of one of the two 6x*Ter* arrays. **d**, One of three independent experiments performed with p6x*Ter*-2Ori. Methods as in Fig. 1b. Note presence of four stall spots in p6x*Ter*-2Ori replicating in presence of wtTus. Double Y stall spots C and C2 and background signal C′ were quantified. Note: shape and size of each area is identical *within* an individual experiment, but varies *between* experiments (see Source Data 3). By considering only double Y stall spots (i.e., in which FR/EBNA1 bypass has occurred), the relative abundance of the double Y stall spots C and C2 are used to estimate the efficiency of the Tus/6x*Ter* replication fork barrier. Let *a* = probability of the 6x*Ter* array blocking the fork and *b* = probability of 6x*Ter* bypass. Then:

$$a+b=1.$$

The probability of the two 6x*Ter* arrays blocking *each* fork on one p6x*Ter*-2Ori plasmid (generating spot C2) is a^2.
The probability of one 6x*Ter* array being blocked and the second array being bypassed (generating spot C) is $2ab$.
Relative densitometry of spots C and C2 (each with subtraction of background C′—Source Data 3) shows that spot C contributes 49.6% and C2 contributes 50.4% (s.e.m. 5.6%).
Therefore:

$$0.496a^2=0.504\times 2ab$$
$$a=0.67$$

Therefore, the estimated efficiency of the Tus/6x*Ter* replication fork block within the *replicating plasmid* is 67%. Note: the efficiency of the Tus/6x*Ter* replication fork block within the *chromosome* is unknown.

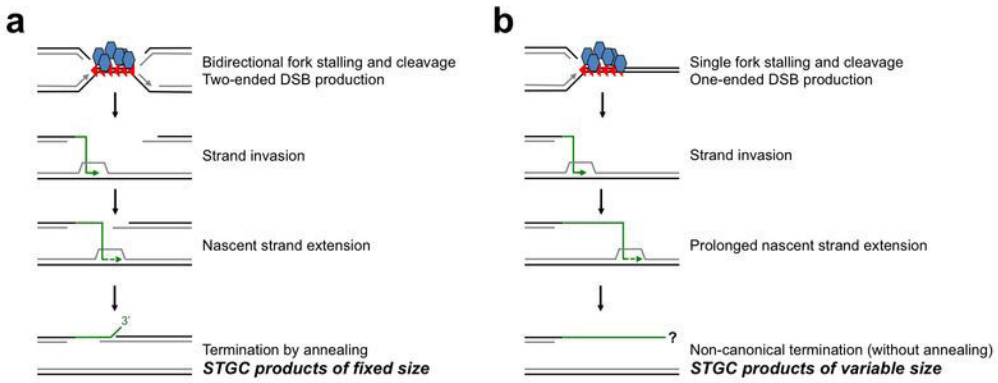

Extended Data Figure 3. Two-ended *vs*. one-ended break repair models of Tus/*Ter*-induced HR

a, Bidirectional fork arrest would provide two DNA ends for sister chromatid recombination. Termination by annealing generates STGC products of a fixed size. Recombining *GFP* elements and HR reporter features other than Tus/*Ter* are not shown. Black strands: parental DNA. Grey strands: newly synthesized DNA. Arrow heads on DNA strands represent DNA synthesis. Blue/grey hexagons: Tus monomers. Red triangles: *Ter* sites. Green line: invading DNA strand. Green dotted line: nascent strand extension. **b**, Unidirectional fork arrest would provide only one DNA end for sister chromatid recombination. Following one-ended invasion of the neighboring sister chromatid, any STGC products could not be terminated by annealing, since there is no homologous second end. Termination by non-canonical mechanisms would generate STGCs of unpredictable/variable size, as in Chandramouly et al[20]. DNA and protein elements labeled as in panel (a).

Note 1: LTGC is not considered in this analysis, since the mechanisms of termination of the major LTGC products are not accessible from the current data.

Note 2: Each model invokes a hypothetical DSB intermediate. Tus/*Ter*-induced HR could be initiated by a template switching mechanism (i.e., without the formation of an *initiating* DSB intermediate). However, the requirement for a homologous second end is not altered by consideration of a template switch model and this second end must be provided by the processing of a second arrested fork (the right-hand fork in panel a).

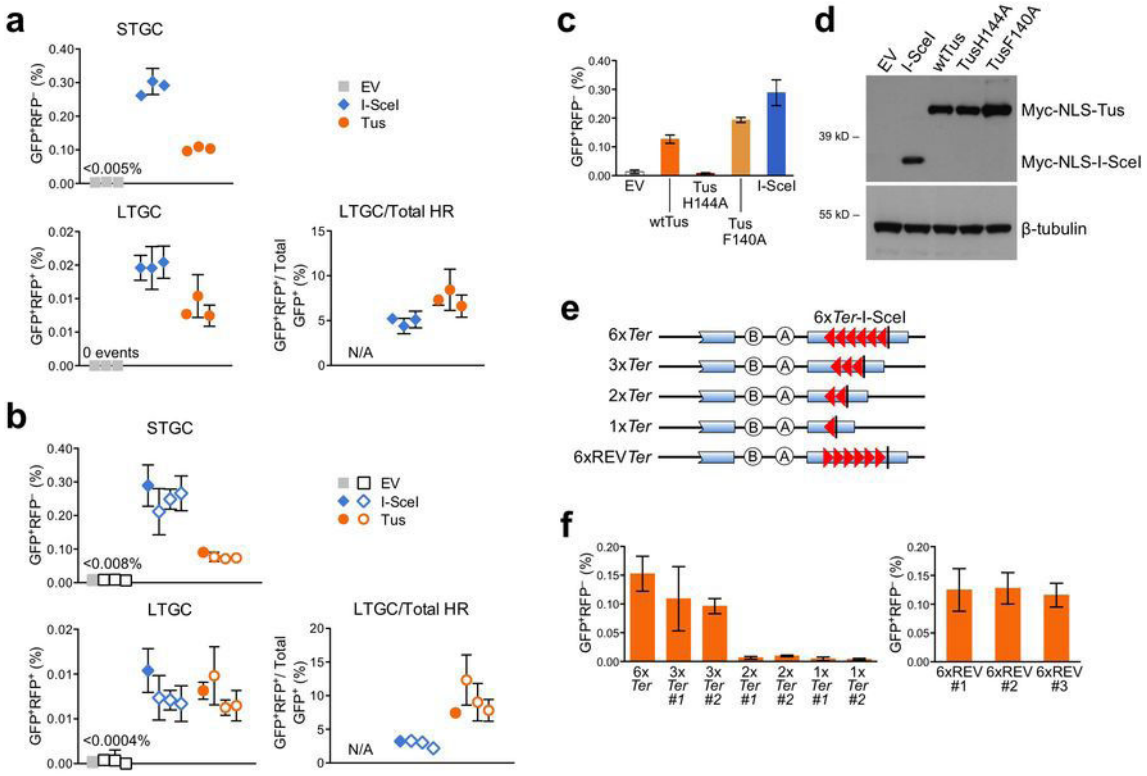

Extended Data Figure 4. Tus/*Ter*-induced HR in *Brca1*$^{fl/BRCT}$ 6x*Ter*/HR cells conforms to an affinity/avidity model

a, Primary data from Fig. 2c, showing directly measured frequencies of background HR, Tus-induced HR and I-SceI-induced HR in three independent *Brca1*$^{fl/BRCT}$ 6x*Ter*/HR reporter clones. Cells were transfected with empty vector (EV; grey squares), myc-NLS-I-SceI (I-SceI; blue diamonds), or myc-NLS-Tus expression vectors (Tus; orange circles). Each point represents the mean of triplicate samples from three independent experiments (i.e., n=3). Error bars: s.e.m. *t*-test of Tus *vs*. EV: STGC P< 0.0001; LTGC P< 0.0001. *t*-test of I-SceI *vs*. EV: STGC P< 0.0001; LTGC P< 0.0001. *t*-test of Tus *vs*. I-SceI: STGC P <0.0001; LTGC P= 0.0018 ; LTGC/Total HR P=0.0186. **b**, Primary data comparing a single *ROSA26* targeted *Brca1*$^{fl/BRCT}$ 6x*Ter*/HR clone with three independently derived clones, each harboring a single intact 6x*Ter*/HR reporter randomly integrated at an unknown locus. Filled symbols: *ROSA26*-targeted clone (as in panel a). Open symbols: data from randomly integrated 6x*Ter*/HR reporter clones. Each point represents the mean of six independent experiments, triplicate replicates for each experiment (i.e., n=6). Error bars: s.e.m. *t*-test of pooled random integrants Tus *vs*. EV: STGC P< 0.0001; LTGC P< 0.0001. *t*-test of pooled random integrants I-SceI *vs*. EV: STGC P< 0.0001; LTGC P< 0.0001. *t*-test of pooled random integrants Tus *vs*. I-SceI: STGC P< 0.0001; LTGC P= 0.3620; LTGC/Total HR P= 0.00012. **c**, Primary data of STGC products observed in *Brca1*$^{fl/BRCT}$ 6x*Ter*/HR cells transfected with empty vector (EV), wtTus, DNA binding defective TusH144A, lock defective TusF140A, or I-SceI. All expression vectors are codon-optimized for mammalian expression and encode N-terminal myc epitope and NLS sequences. Each column represents the mean of six independent experiments (i.e., n=6). Error bars: s.e.m. *t*-test of wtTus *vs*. EV: P= 0.0002; wtTus *vs*. TusH144A: P= 0.0004; wtTus *vs*. TusF140A: P= 0.0042; wtTus

vs. I-SceI: P= 0.0139; TusH144A *vs*. EV: P= 0.4406; TusF140A *vs*. EV: P< 0.0001; TusF140A *vs*. TusH144A: P< 0.0001; TusF140A *vs*. I-SceI: P= 0.0888. **d**, Myc-tagged protein abundance in transfected *Brca1*$^{fl/BRCT}$ 6x*Ter*-HR cells: EV: empty vector. Other lanes as marked. Lower panel: beta-tubulin loading control. (Source Data 4) **e**, Cartoons of the *Ter*/HR reporter constructs assayed in panel (f). **f**, Frequencies of Tus-induced STGC in *Brca1*$^{fl/BRCT}$ cells carrying single copy, *ROSA26*-targeted *Ter*/HR reporters shown in panel (e). Left: HR in 6x*Ter*, 3x*Ter*, 2x*Ter* and 1x*Ter* HR reporters, as shown. Right: HR in three independently derived clones carrying single copy, *ROSA26*-targeted 6xREV*Ter* HR reporters. Each column represents the mean of three independent experiments (i.e., n=3). Error bars: s.e.m. *t*-test of 6x*Ter vs*. 3x*Ter#1*: P= 0.2604; 6x*Ter vs*. 3x*Ter#2*: P= 0.5192; 6x*Ter vs*. 2x*Ter#1*: P= 0.0547; 6x*Ter vs*. 2x*Ter#2*: P= 0.0524; 6x*Ter vs*. 1x*Ter#1*: P= 0.0507; 6x*Ter vs*. 1x*Ter#2*: P= 0.0507; 3x*Ter#1 vs*. 3x*Ter#2*: P= 0.8291; 3x*Ter#1 vs*. 2x*Ter#1*: P= 0.0650; 3x*Ter#1 vs*. 2x*Ter#2*: P= 0.0606; 3x*Ter#1 vs*. 1x*Ter#1*: P= 0.0576; 3x*Ter#1 vs*. 1x*Ter#2*: P= 0.0574; 3x*Ter#2 vs*. 2x*Ter#1*: P= 0.1832; 3x*Ter#2 vs*. 2x*Ter#2*: P= 0.1748; 3x*Ter#2 vs*. 1x*Ter#1*: P= 0.1677; 3x*Ter#2 vs*. 1x*Ter#2*: P= 0.1697.
By one-way ANOVA (Analysis of Variance) test used to compare more than three sets of data, the trend in HR from 6x−1x p=0.0012.

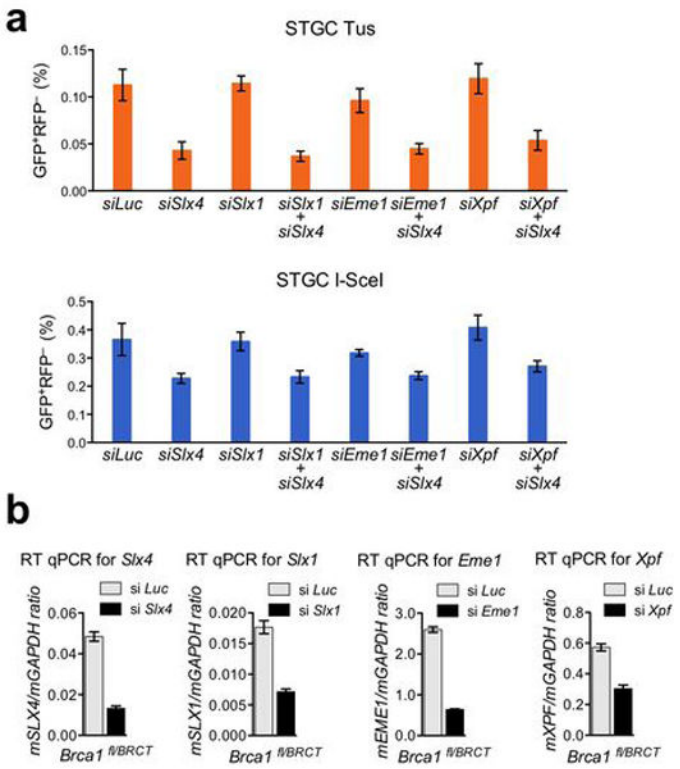

Extended Data Figure 5. Slx4/FancP depletion suppresses Tus/*Ter*-induced HR

a, Frequencies of STGC in *Brca1*$^{fl/BRCT}$ 6x*Ter*-HR cells co-transfected with Tus (orange) or I-SceI (blue) and with either control Luciferase siRNA (si *Luc*), Slx4 SMARTpool (si *Slx4*), Slx1 SMARTpool (si *Slx1*), Slx1 and Slx4 SMARTpools (si Slx1 si *Slx4*), Eme1 SMARTpool (si *Eme1*), Eme1 and Slx4 SMARTpools (si *Eme1* si *Slx4*), Xpf SMARTpool (si *Xpf*), Xpf and Slx4 SMARTpools (si *Xpf* si *Slx4*). Each column represents the mean of

triplicate samples from four independent experiments for each clone (i.e., n=4). Error bars: s.e.m. Tus-induced HR: *t*-test of si *Slx4 vs*. si Luc: P= 0.0219; si *Slx4 vs*. si Slx1: P= 0.0012; si *Slx4 vs*. si *Slx4+1*: P= 0.5983; si *Slx4 vs*. si *Eme1*: P= 0.0171; si *Slx4 vs*. si *Slx4* +si *Eme1*: P= 0.8721; si *Slx4 vs*. si *Xpf*: P= 0.0098; si *Slx4 vs*. si *Slx4*+ si *Xpf*: P= 0.4711; si *Slx1 vs*. si Luc: P= 0.9332; si *Eme1 vs*. si Luc: P= 0.4631; si *Xpf vs*. si Luc: P= 0.7818; si *Slx4+1 vs*. si Luc: P= 0.0155; si *Slx4*+si *Eme1 vs*. si Luc: P= 0.0215; si *Slx4* + si *Xpf vs*. si Luc: P= 0.0305. I-SceI-induced HR: *t*-test of si *Slx4 vs*. si Luc: P= 0.0907; si *Slx4 vs*. si Slx1: P= 0.0195; si *Slx4 vs*. si *Slx4+1*: P= 0.4897; si *Slx4 vs*. si *Eme1*: P= 0.0568; si *Slx4 vs*. si *Slx4* +si *Eme1*: P= 0.3411; si *Slx4 vs*. si *Xpf*: P= 0.0745; si *Slx4 vs*. si *Slx4*+ si *Xpf*: P= 0.2726; si *Slx1 vs*. si Luc: P= 0.9198; si *Eme1 vs*. si Luc: P= 0.3349; si *Xpf vs*. si Luc: P= 0.9217; si *Slx4+1 vs*. si Luc: P= 0.1521; si *Slx4*+si *Eme1 vs*. si Luc: P= 0.2864; si *Slx4* + si *Xpf vs*. si Luc: P= 0.2063. **b**, RT qPCR analysis of mRNA exon boundaries for *Slx4, Slx1, Eme1,* and *Xpf* mRNA in siRNA-SMARTpool-treated cells used in panel (a).

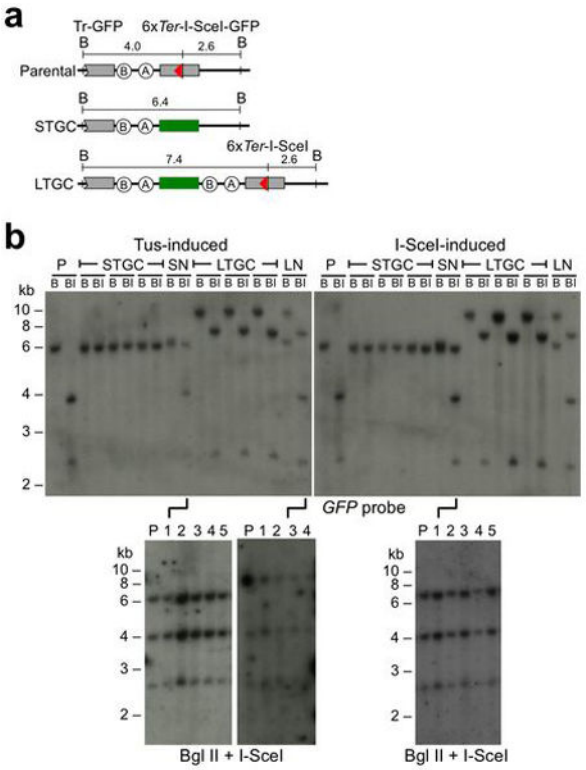

Extended Data Figure 6. Southern blot analysis of Tus/*Ter*- and I-SceI-induced HR products in *Brca1*$^{\Delta/BRCT}$ 6x*Ter*/HR cells

a, Structure of the 6x*Ter*/HR parental reporter, and major STGC or LTGC HR products (assuming two-ended breaks). Elements as shown in Fig. 2a. **b**, Southern blot analysis of Tus-induced and I-SceI induced HR products in *Brca1*$^{\Delta/BRCT}$ 6x*Ter*-HR cells. P: un-rearranged reporter; STGC and LTGC as shown. SN: STGC accompanied nondisjunction with retention of parental donor reporter; LN: LTGC accompanied nondisjunction with retention of parental donor reporter. B: BglII digest. BI: BglII + I-SceI digest. Membranes probed with full length *GFP* cDNA. Panels underneath two SN events and one LN event

show that re-cloning does not separate the two reporters, confirming that the cell contains two copies of the reporter (consistent with nondisjunction).

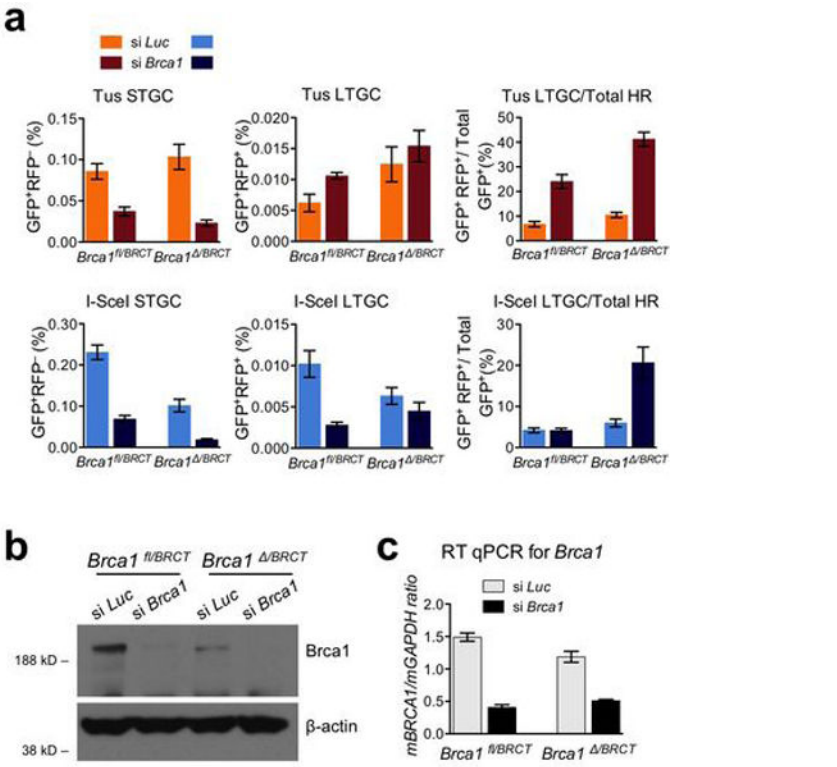

Extended Data Figure 7. Brca1 contributes quantitatively and qualitatively to HR at stalled replication forks

a, Frequencies of Tus-induced and I-SceI-induced HR in *Brca1*$^{fl/BRCT}$ and *Brca1*$^{\Delta/BRCT}$ 6x*Ter*/HR cells transiently co-transfected with Tus, or I-SceI and with either control Luciferase siRNA (si *Luc*) or Brca1 SMARTpool (si *Brca1*). Each column represents the mean of triplicate samples for each independent clone from seven independent experiments (i.e., n=7). Error bars: s.e.m. Tus-induced HR, *Brca1*$^{fl/BRCT}$ cells, *t*-test si *Brca1 vs*. si *Luc*: STGC: P= 0.0013; LTGC: P= 0.0206; LTGC/total HR: P= 0.0003; *Brca1*$^{\Delta/BRCT}$ cells, si *Brca1 vs*. si *Luc*: STGC: P= 0.0016; LTGC: P= 0.4558; LTGC/total HR: P< 0.0001. I-SceI-induced HR, *Brca1*$^{fl/BRCT}$ cells, *t*-test si *Brca1 vs*. si *Luc*: STGC: P< 0.0001; LTGC: P= 0.0033; LTGC/total HR: P= 0.9214; *Brca1*$^{\Delta/BRCT}$ cells, si *Brca1 vs*. si *Luc*: STGC: P= 0.0013; LTGC: P= 0.2348; LTGC/total HR: P= 0.0071. **b**, Brca1 protein levels and beta-actin loading control in *Brca1*$^{fl/BRCT}$ and *Brca1*$^{\Delta/Exon11}$ in siRNA-treated cells as shown. **c**, RT qPCR analysis of *Brca1* mRNA in siRNA-treated cells as shown. (Source Data 6.)

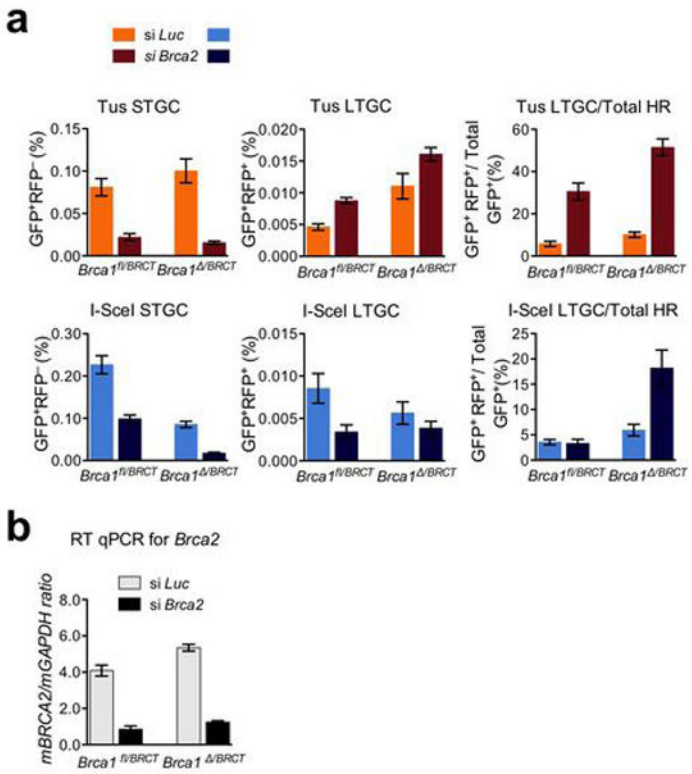

Extended Data Figure 8. Brca2 contributes quantitatively and qualitatively to HR at stalled replication forks

a, Frequencies of Tus-induced and I-SceI-induced HR in *Brca1*$^{fl/BRCT}$ and *Brca1*$^{\Delta/BRCT}$ 6x*Ter*/HR cells transiently co-transfected with Tus, or I-SceI and with either control Luciferase siRNA (si *Luc*) or Brca2 SMARTpool (si *Brca2*). Each column represents the mean of triplicate samples for each independent clone from five independent experiments (i.e., n=5). Error bars: s.e.m. Tus-induced HR, *Brca1*$^{fl/BRCT}$ cells, *t*-test si *Brca2 vs*. si *Luc*: STGC: P= 0.0031; LTGC: P= 0.0007; LTGC/total HR: P= 0.0042; *Brca1*$^{\Delta/BRCT}$ cells, si *Brca2 vs*. si *Luc*: STGC: P= 0.0040; LTGC: P= 0.0013; LTGC/total HR: P= 0.0006. I-SceI-induced HR, *Brca1*$^{fl/BRCT}$ cells, *t*-test si *Brca2 vs*. si *Luc*: STGC: P= 0.0028; LTGC: P= 0.0456; LTGC/total HR: P= 0.7945; *Brca1*$^{\Delta/BRCT}$ cells, si *Brca2 vs*. si *Luc*: STGC: P= 0.0010; LTGC: P= 0.2926; LTGC/total HR: P= 0.0316. **b**, RT qPCR analysis of *Brca2* mRNA in siRNA-treated cells as shown.

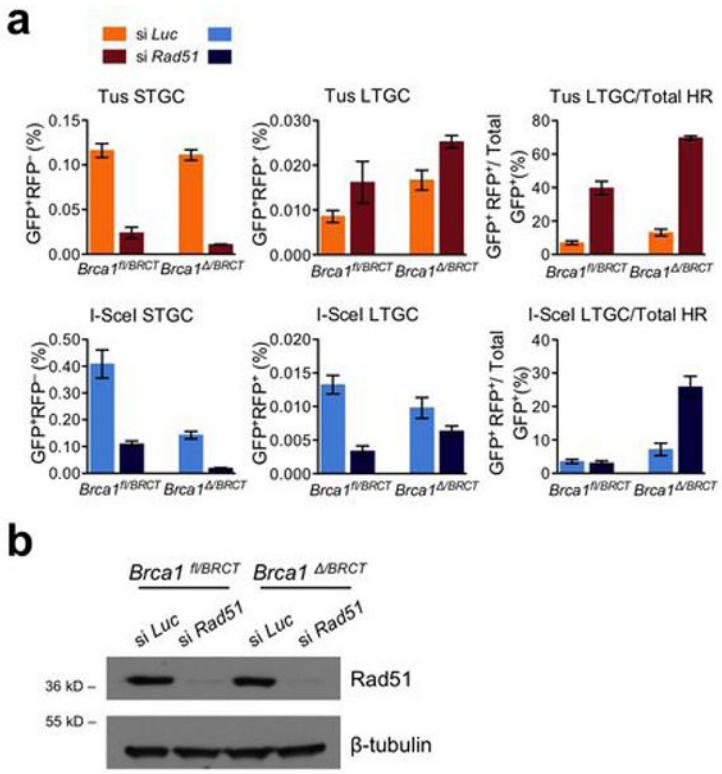

Extended Data Figure 9. Rad51 contributes quantitatively and qualitatively to HR at stalled replication forks

a, Frequencies of Tus-induced and I-SceI-induced HR in *Brca1*$^{fl/BRCT}$ and *Brca1*$^{\Delta/BRCT}$ 6x*Ter*/HR cells transiently co-transfected with Tus, or I-SceI and with either control Luciferase siRNA (si *Luc*) or Rad51 SMARTpool (si *Rad51*). Each column represents the mean of triplicate samples for each independent clone from seven independent experiments for *Brca1*$^{fl/BRCT}$ (i.e., n=7) and four independent experiments for *Brca1*$^{\Delta/BRCT}$ cells (i.e., n=4). Error bars: s.e.m. Tus-induced HR, *Brca1*$^{fl/BRCT}$ cells, *t*-test si *Rad51 vs*. si *Luc*: STGC: P< 0.0001; LTGC: P= 0.1578; LTGC/total HR: P= 0.0002; *Brca1*$^{\Delta/BRCT}$ cells, si *Rad51 vs*. si *Luc*: STGC: P= 0.0010; LTGC: P= 0.0676; LTGC/total HR: P< 0.0001. I-SceI-induced HR, *Brca1*$^{fl/BRCT}$ cells, *t*-test si *Rad51 vs*. si *Luc*: STGC: P= 0.0014; LTGC: P= 0.0002; LTGC/total HR: P= 0.6216; *Brca1*$^{\Delta/BRCT}$ cells, si *Rad51 vs*. si *Luc*: STGC: P= 0.0068; LTGC: P= 0.2064; LTGC/total HR: P= 0.0186. **b**, Rad51 protein levels and beta-tubulin loading control in *Brca1*$^{fl/BRCT}$ and *Brca1*$^{\Delta/BRCT}$ siRNA-treated cells as shown. (Source Data 8.)

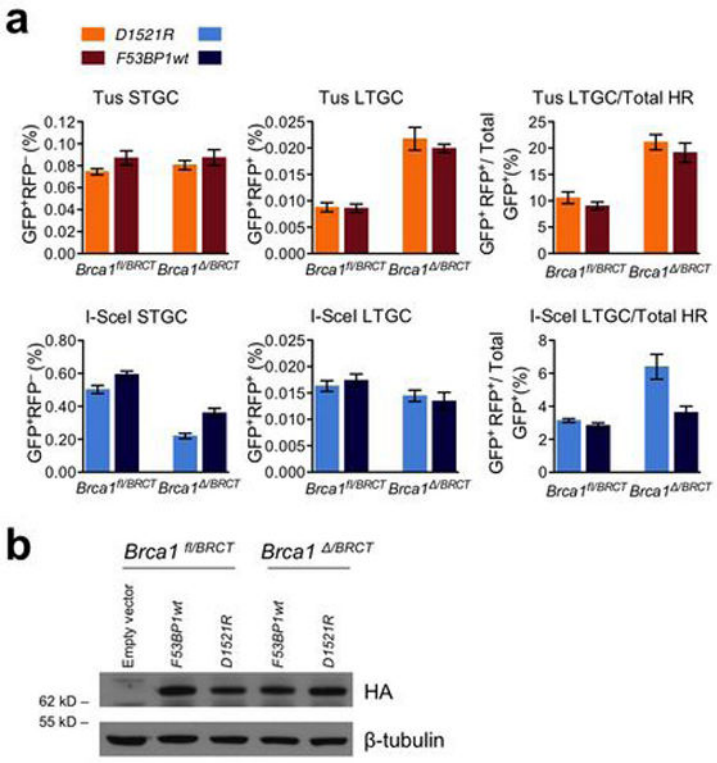

Extended Data Figure 10. Effect of 53BP1 inhibition on Tus/*Ter*-induced HR

a, Frequencies of Tus-induced and I-SceI-induced HR in *Brca1*$^{fl/BRCT}$ and *Brca1*$^{\Delta/BRCT}$ 6x*Ter*/HR cells transiently co-transfected with Tus or I-SceI expression vectors and with either F53BP1 D1521R fragment (D1521R; non-chromatin-binding negative control for "dominant negative" 53BP1 fragment) or "dominant negative" F53BP1wt fragment (F53BP1wt). Each column represents the mean of triplicate samples for each independent clone from five independent experiments (i.e., n=5). Error bars: s.e.m. Tus-induced HR, *Brca1*$^{fl/BRCT}$ cells, *t*-test D1521R *vs*. F53BP1wt: STGC: P= 0.1818; LTGC: P= 0.9005; LTGC/total HR: P= 0.3570; *Brca1*$^{\Delta/BRCT}$ *cells*, *t*-test D1521R *vs*. F53BP1wt: STGC: P= 0.5008; LTGC: P= 0.5375; LTGC/total HR: P= 0.4921. I-SceI-induced HR, *Brca1*$^{fl/BRCT}$ cells, *t*-test D1521R *vs*. F53BP1wt: STGC: P= 0.0442; LTGC: P= 0.5739 ; LTGC/total HR: P= 0.2250; *Brca1*$^{\Delta/BRCT}$ *cells*, *t*-test D1521R *vs*. F53BP1wt: STGC: P= 0.0086; LTGC: P= 0.6888; LTGC/total HR: P= 0.0328. Tus-induced LTGC/total HR, *Brca1*$^{fl/BRCT}$ vs. *Brca1*$^{\Delta/BRCT}$ *cells*, *t*-test F53BP1wt: 0.0064; *Brca1*$^{fl/BRCT}$ vs. *Brca1*$^{\Delta/BRCT}$ *cells*, *t*-test D1521R: 0.0014; I-SceI-induced LTGC/total HR, *Brca1*$^{fl/BRCT}$ vs. *Brca1*$^{\Delta/BRCT}$ *cells*, *t*-test F53BP1wt: 0.1556; *Brca1*$^{fl/BRCT}$ vs. *Brca1*$^{\Delta/BRCT}$ *cells*, *t*-test D1521R: 0.0208. **b**, Abundance of 53BP1 fragments, and beta-tubulin (loading control) in treated *Brca1*$^{fl/BRCT}$ and *Brca1*$^{\Delta/BRCT}$ 6x*Ter*/HR reporter ES cells in (a). (Source Data 9.)

Acknowledgments

We thank B Michel for reagents and advice; D Livingston, K Marians, J Walter, I Hickson, S Powell, V Zakian and members of the Scully lab for helpful discussions; I Hickson and S Powell for sharing their unpublished data on Tus/*Ter* replication blocks in eukaryotes; R Baer for antibodies and A Ashworth for *Brca1* conditional ES cell line 11CO/47T. This work was supported by NIH grants R01CA095175, R01GM073894 and R21CA144017 (to R.S.).

N.A.W. was supported by an NIH/NCI postdoctoral fellowship (5T32 CA081156-10) and an ACS postdoctoral research fellowship (PF-12-248-01-DMC). C.F. was supported by NIH grant RO1GM26938 (to V.A.Z.).

References

1. Ciccia A, Elledge SJ. The DNA damage response: making it safe to play with knives. Mol Cell. 2010; 40:179–204. [PubMed: 20965415]
2. Nagaraju G, Scully R. Minding the gap: The underground functions of BRCA1 and BRCA2 at stalled replication forks. DNA Repair (Amst). 2007
3. Hastings PJ, Ira G, Lupski JR. A microhomology-mediated break-induced replication model for the origin of human copy number variation. PLoS Genetics. 2009; 5:e1000327. [PubMed: 19180184]
4. Kowalczykowski SC. Initiation of genetic recombination and recombination-dependent replication. Trends Biochem Sci. 2000; 25:156–165. [PubMed: 10754547]
5. Cox MM, et al. The importance of repairing stalled replication forks. Nature. 2000; 404:37–41. [PubMed: 10716434]
6. Michel B, Grompone G, Flores MJ, Bidnenko V. Multiple pathways process stalled replication forks. Proc Natl Acad Sci U S A. 2004; 101:12783–12788. [PubMed: 15328417]
7. Lambert S, et al. Homologous recombination restarts blocked replication forks at the expense of genome rearrangements by template exchange. Mol Cell. 2010; 39:346–359. [PubMed: 20705238]
8. Carr AM, Lambert S, Replication Stress-Induced. Genome Instability: The Dark Side of Replication Maintenance by Homologous Recombination. J Mol Biol. 2013
9. Scully R, Livingston DM. In search of the tumour-suppressor functions of BRCA1 and BRCA2. Nature. 2000; 408:429–432. [PubMed: 11100717]
10. Lomonosov M, Anand S, Sangrithi M, Davies R, Venkitaraman AR. Stabilization of stalled DNA replication forks by the BRCA2 breast cancer susceptibility protein. Genes Dev. 2003; 17:3017–3022. [PubMed: 14681210]
11. Pathania S, et al. BRCA1 is required for postreplication repair after UV-induced DNA damage. Mol Cell. 2011; 44:235–251. [PubMed: 21963239]
12. Schlacher K, et al. Double-strand break repair-independent role for BRCA2 in blocking stalled replication fork degradation by MRE11. Cell. 2011; 145:529–542. [PubMed: 21565612]
13. Amin AA, Hurwitz J. Polar arrest of the simian virus 40 tumor antigen-mediated replication fork movement in vitro by the tus protein-terB complex of *Escherichia coli*. J Biol Chem. 1992; 267:18612–18622. [PubMed: 1326530]
14. Hill TM, Marians KJ. *Escherichia coli* Tus protein acts to arrest the progression of DNA replication forks in vitro. Proc Natl Acad Sci USA. 1990; 87:2481–2485. [PubMed: 2181438]
15. Bidnenko V, Ehrlich SD, Michel B. Replication fork collapse at replication terminator sequences. EMBO J. 2002; 21:3898–3907. [PubMed: 12110601]
16. Mulcair MD, et al. A molecular mousetrap determines polarity of termination of DNA replication in E. coli. Cell. 2006; 125:1309–1319. [PubMed: 16814717]
17. Dhar SK, et al. Replication from oriP of Epstein-Barr virus requires human ORC and is inhibited by geminin. Cell. 2001; 106:287–296. [PubMed: 11509178]
18. Kirchmaier AL, Sugden B. Plasmid maintenance of derivatives of oriP of Epstein-Barr virus. J Virol. 1995; 69:1280–1283. [PubMed: 7815506]
19. Gahn TA, Schildkraut CL. The Epstein-Barr virus origin of plasmid replication, oriP, contains both the initiation and termination sites of DNA replication. Cell. 1989; 58:527–535. [PubMed: 2547525]
20. Chandramouly G, et al. BRCA1 and CtIP suppress long-tract gene conversion between sister chromatids. Nat Commun. 2013; 4:2404. [PubMed: 23994874]
21. Raschle M, et al. Mechanism of replication-coupled DNA interstrand crosslink repair. Cell. 2008; 134:969–980. [PubMed: 18805090]
22. Castor D, et al. Cooperative control of holliday junction resolution and DNA repair by the SLX1 and MUS81-EME1 nucleases. Mol Cell. 2013; 52:221–233. [PubMed: 24076219]

23. Garner E, Kim Y, Lach FP, Kottemann MC, Smogorzewska A. Human GEN1 and the SLX4-associated nucleases MUS81 and SLX1 are essential for the resolution of replication-induced Holliday junctions. Cell Rep. 2013; 5:207–215. [PubMed: 24080495]
24. Johnson RD, Jasin M. Sister chromatid gene conversion is a prominent double-strand break repair pathway in mammalian cells. EMBO J. 2000; 19:3398–3407. [PubMed: 10880452]
25. Nagaraju G, Odate S, Xie A, Scully R. Differential regulation of short- and long-tract gene conversion between sister chromatids by Rad51C. Mol Cell Biol. 2006; 26:8075–8086. [PubMed: 16954385]
26. Huber LJ, et al. Impaired DNA damage response in cells expressing an exon 11-deleted murine Brca1 variant that localizes to nuclear foci. Mol Cell Biol. 2001; 21:4005–4015. [PubMed: 11359908]
27. Xu X, et al. Conditional mutation of *Brca1* in mammary epithelial cells results in blunted ductal morphogenesis and tumour formation. Nature Genet. 1999; 22:37–43. [PubMed: 10319859]
28. Llorente B, Smith CE, Symington LS. Break-induced replication: what is it and what is it for? Cell Cycle. 2008; 7:859–864. [PubMed: 18414031]
29. Saini N, et al. Migrating bubble during break-induced replication drives conservative DNA synthesis. Nature. 2013; 502:389–392. [PubMed: 24025772]
30. Follonier C, Lopes M. Combined bidimensional electrophoresis and electron microscopy to study specific plasmid DNA replication intermediates in human cells. Methods Mol Biol. 2014; 1094:209–219. [PubMed: 24162990]
31. Chandramouly G, et al. BRCA1 and CtIP suppress long-tract gene conversion between sister chromatids. Nat Commun. 2013; 4:2404. [PubMed: 23994874]
32. Xie A, et al. Distinct roles of chromatin-associated proteins MDC1 and 53BP1 in mammalian double-strand break repair. Mol Cell. 2007; 28:1045–1057. [PubMed: 18158901]
33. Xie A, et al. Control of sister chromatid recombination by histone H2AX. Mol Cell. 2004; 16:1017–1025. [PubMed: 15610743]
34. Puget N, Knowlton M, Scully R. Molecular analysis of sister chromatid recombination in mammalian cells. DNA Repair (Amst). 2005; 4:149–161. [PubMed: 15590323]
35. Follonier C, Lopes M. Combined bidimensional electrophoresis and electron microscopy to study specific plasmid DNA replication intermediates in human cells. Methods Mol Biol. 2014; 1094:209–219. [PubMed: 24162990]

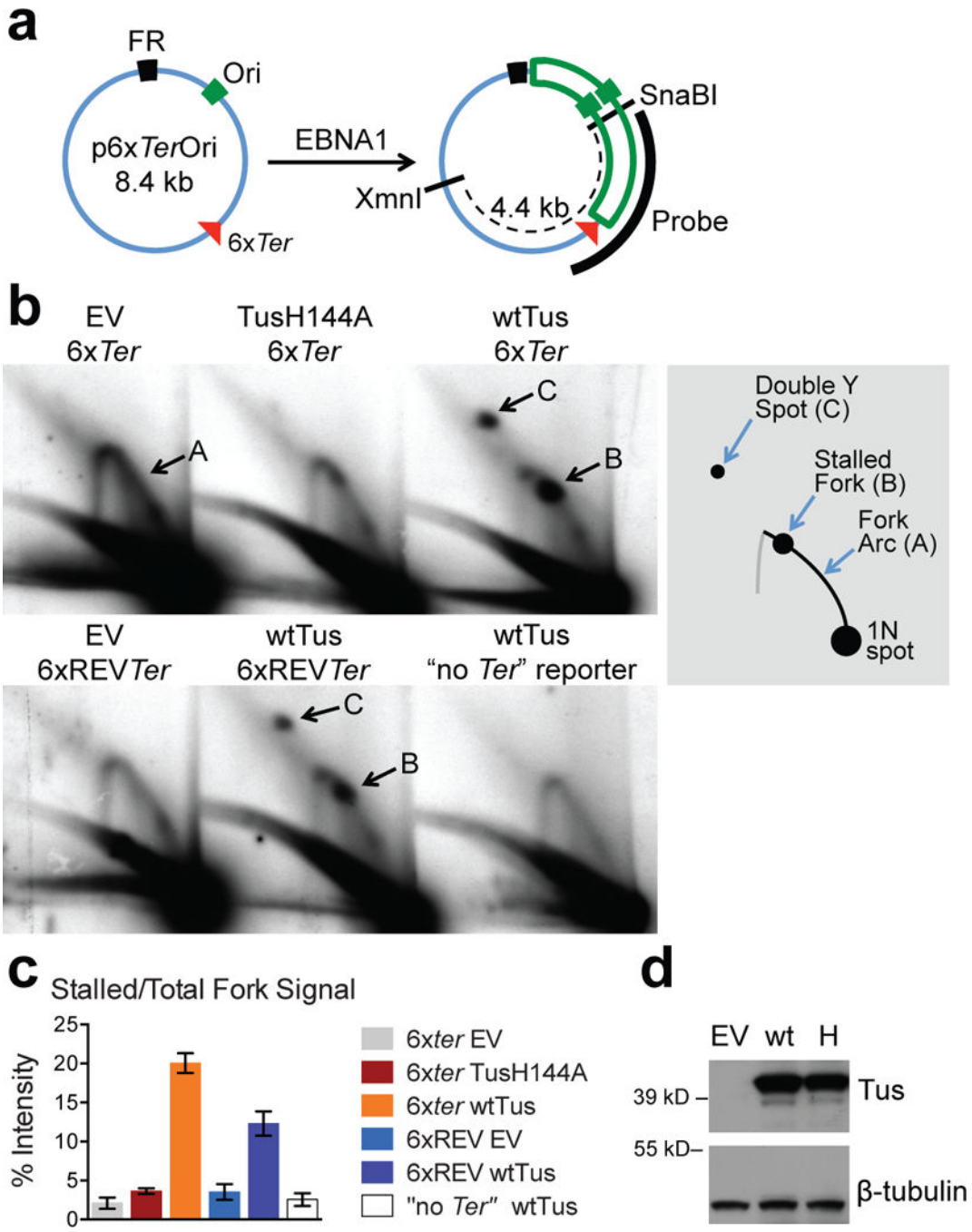

Figure 1. Tus/*Ter*-induced replication fork stalling in mammalian cells

(a) EBNA1-driven plasmid replication. Ori: EBNA1-binding origin of replication. EBNA1-binding FR repeats impede counterclockwise fork. Red triangle: 6x*Ter* array (vertex: non-permissive end). Southern blotting probe shown. (b) Plasmid replication intermediates in 293E cells transiently transfected with 6x*Ter*-containing plasmids or "no *Ter*" control, co-transfected with empty vector (EV), TusH144A or wtTus. Samples from one experiment (Source Data 1). DNA digested with XmnI+SnaBI and analyzed by 2DGE/Southern blotting. 6xREV*Ter*: clockwise fork encounters permissive end of *Ter*. Cartoon: Arc "A":

replication fork. Spot “B”: Tus/*Ter*-stalled clockwise fork. Spot “C” : Bidirectional fork arrest (“Double Y”) at Tus/6x*Ter*, reflecting incomplete replication block at FR[19]. (c) Stall spot “B” quantitation, n=5 (Source Data 1). Error bars: s.e.m.: *t*-test 6x*Ter* wtTus *vs*. any other, P<0.01. 6xREV*Ter* wtTus *vs*. any other, P<0.01. 6x*Ter* TusH144A *vs*. 6x*Ter* EV, P<0.03. (d) Upper panel: Anti-myc immunoblot of 293E cells expressing empty vector (EV), wtTus (wt) or TusH144A (H). Lower panel: ß tubulin loading control.

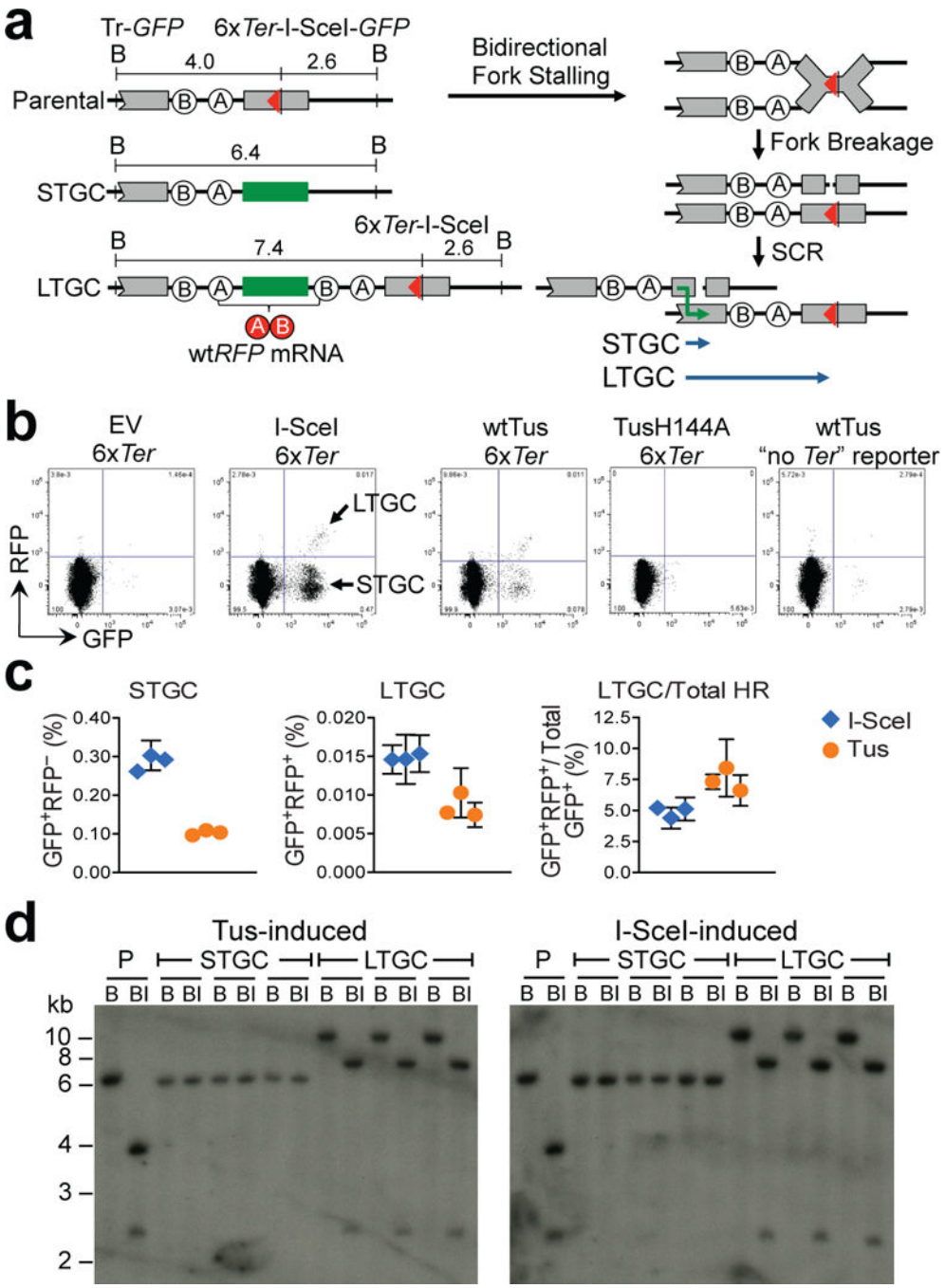

Figure 2. Tus/*Ter*-induced homologous recombination in mammalian cells

(a) 6x*Ter*-HR reporter and major HR products (assuming 2-ended breaks). STGC/LTGC: short/long tract gene conversion. LTGC generates *wtRFP* expression through RNA splicing. Grey boxes: mutant *GFP*. Green box: wt*GFP*. Circles A and B: 5′ and 3′ artificial *RFP* exons. Tr-*GFP*: 5′ truncated *GFP*. Red triangle: 6x*Ter* array adjacent to I-SceI site. B: BglII; *GFP*-hybridizing fragment sizes in kb. Bidirectional fork stalling triggers SCR. Green arrow: strand exchange. (b) FACS data of *Brca1*$^{fl/BRCT}$ 6x*Ter*-HR cells transfected with empty vector (EV), I-SceI, wtTus or TusH144A. "no *Ter*" reporter: *Brca1*$^{fl/BRCT}$ cells

carrying *ROSA26*-targeted HR reporter lacking *Ter* array[20]. (c) I-SceI- and Tus-induced HR (blue diamonds and orange circles, respectively) in three independent *Brca1*$^{fl/BRCT}$ clones. Mean of triplicate samples, n=3. Error bars: s.e.m. *t*-test LTGC/Total HR, I-SceI *vs*. Tus: P=0.0186. (d) Southern blot analysis of Tus- and I-SceI-induced HR in *Brca1*$^{fl/BRCT}$ 6x*Ter*-HR cells (*GFP* probe). P: parental reporter. B: BglII digest. BI: BglII+I-SceI digest.

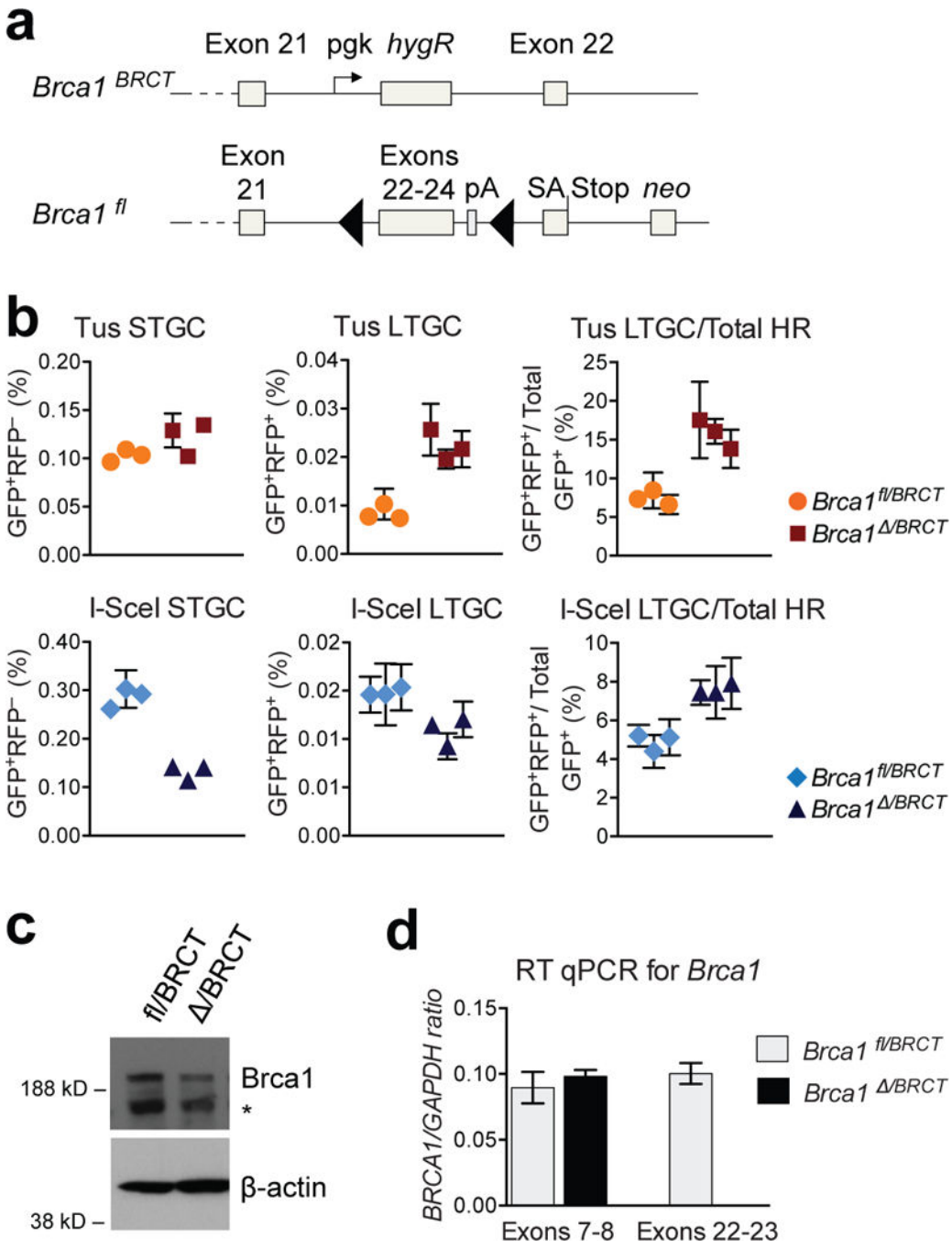

Figure 3. The Brca1 tandem BRCT repeat regulates Tus/*Ter*-induced HR

(a) *Brca1* gene in *Brca1*$^{fl/BRCT}$ ES cells. *Brca1*^{BRCT} encodes truncated protein. Cre converts *Brca*^{fl} to exon 22–24-deleted *Brca1*$^{\Delta}$ allele. Grey boxes: *Brca1* exons; black triangles: *loxP* sites; pA: polyadenylation signal. SA: splice acceptor. *neo:* neomycin resistance gene. pgk: phosphoglycerate kinase promoter. (b) Tus- and I-SceI-induced HR in *Brca1*$^{fl/BRCT}$ and *Brca1*$^{\Delta/BRCT}$ 6x*Ter*-HR cells (three independent clones each). Mean of triplicate samples, n=4. Error bars: s.e.m. *t*-test *Brca1*$^{fl/BRCT}$ *vs. Brca1*$^{\Delta/BRCT}$ in all 6 panels P<0.05. (c) Upper panel: endogenous Brca1 immunoblot in *Brca1*$^{fl/BRCT}$ and *Brca1*$^{\Delta/BRCT}$ ES cells. *:

background band. Lower panel: ß-actin loading control. (Source Data 5.) (d) RT qPCR for *Brca1* mRNA. Exon 22-23 is deleted in *Brca1*$^{\Delta/BRCT}$ cells.

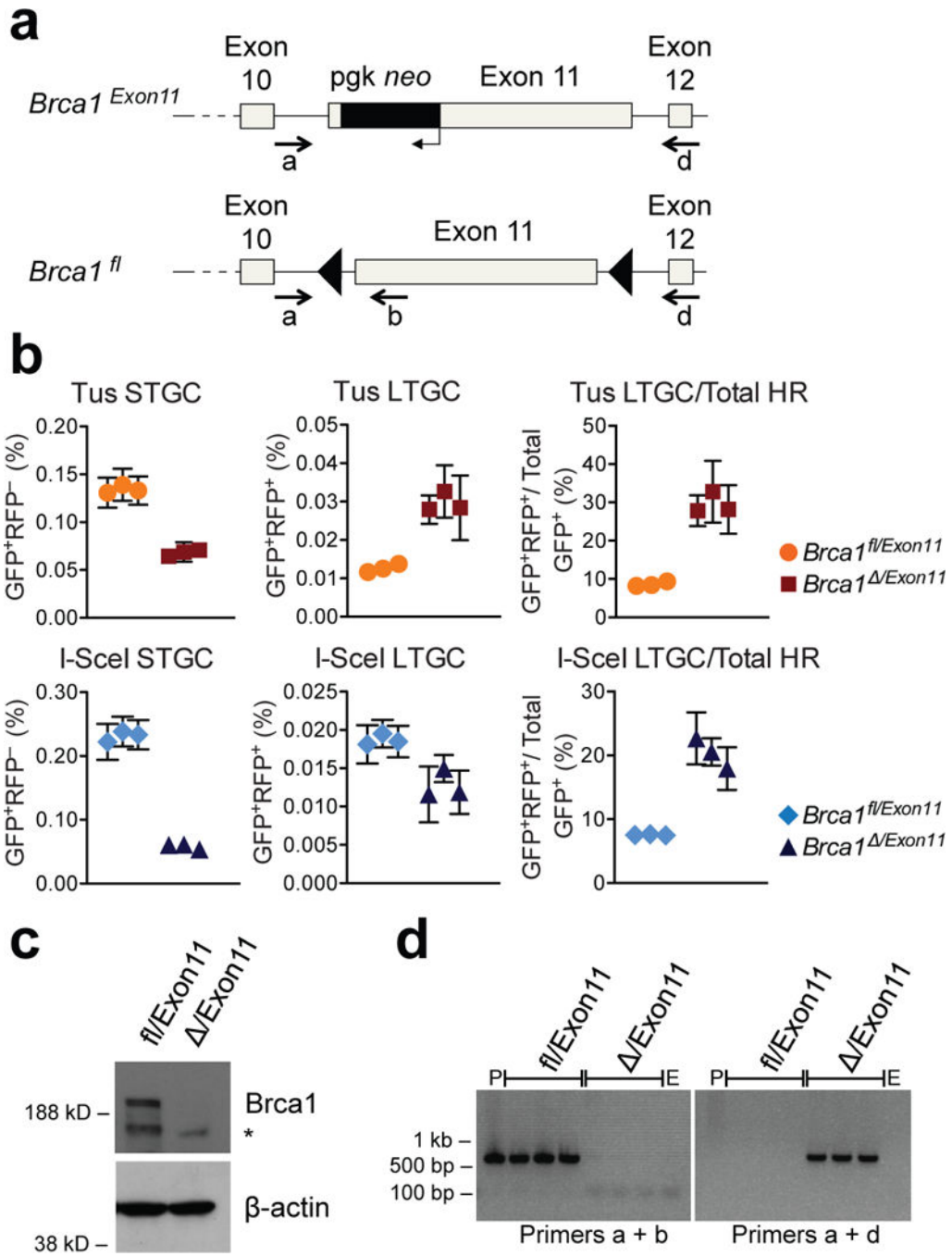

Figure 4. *Brca1* Exon11 regulates Tus/*Ter*-induced HR

(a) *Brca1* gene in $Brca1^{fl/Exon11}$ ES cells. $Brca1^{Exon11}$ encodes Δexon11 product. Cre converts $Brca1^{fl}$ to exon11-deleted $Brca1^{\Delta}$ allele. Symbols as in Fig. 3. PCR primers a, b, and d shown. (b) Tus- and I-SceI-induced HR in $Brca1^{fl/Exon11}$ and $Brca1^{\Delta/Exon11}$ 6x*Ter*-HR cells (three independent clones each). Mean of triplicate samples, n=4. Error bars: s.e.m. *t*-test $Brca1^{fl/Exon11}$ *vs.* $Brca1^{\Delta/Exon11}$, in all 6 panels P<0.005. (c) Upper panel: endogenous Brca1 immunoblot in $Brca1^{fl/Exon11}$ and $Brca1^{\Delta/Exon11}$ ES cells. *: background band. Lower panel: ß-actin loading control. (Source Data 7.) (d) PCR genotyping of $Brca1^{fl/Exon11}$ and

Brca1$^{\Delta/\text{Exon11}}$ clones from panel b. P: untargeted *Brca1*$^{\text{fl/Exon11}}$. E: “empty” (no DNA) control. *Brca1*$^{\text{fl}}$ product: 531 bp. *Brca1*$^{\Delta}$ product: 621 bp.